ACCSCIENCE PUBLISHING

International Journal of Bioprinting

RESEARCH ARTICLE

Rapid 3D reconstruction in fetal ultrasound imaging using artificial intelligence and medical 3D printing

Wenjuan Zhang[1†], Jiahe Liang[2,3,4†], Linbin Lai[1†], Zewen Zhang[1], Yitong Guo[2†], Na Hou[2†], Zekai Zhang[2], Zhuojun Mao[2], Tiesheng Cao[2], Yu Li[5], Lijun Yuan[2*], and Airong Qian[1*]

[1]Xi'an Key Laboratory of Special Medicine and Health Engineering, School of Life Sciences, Northwestern Polytechnical University, Xi'an, Shaanxi, China

[2]Department of Ultrasound Diagnosis, Tangdu Hospital, Fourth Military Medical University, Xi'an, Shaanxi, China

[3]State Key Laboratory for Manufacturing Systems Engineering, Xi'an Jiaotong University, Xi'an, Shaanxi, China

[4]NMPA Key Laboratory for Research and Evaluation of Additive Manufacturing Medical Devices, Xi'an Jiaotong University, Xi'an, Shaanxi, China

[5]Xi'an Key Laboratory of Stem Cell and Regenerative Medicine, Institute of Medical Research, Northwestern Polytechnical University, Xi'an, Shaanxi, China

[†]These authors contributed equally to this work.

***Corresponding authors:**
Lijun Yuan
(yuanlj@fmmu.edu.cn)

Airong Qian
(qianair@nwpu.edu.cn)

Citation: Zhang W, Liang J, Lai L, *et al*. Rapid 3D reconstruction in fetal ultrasound imaging using artificial intelligence and medical 3D printing. *Int J Bioprint*. 2025;11(4):242-255. doi: 10.36922/IJB025200192

Received: May 12, 2025
Revised: May 30, 2025
Accepted: June 1, 2025
Published online: June 1, 2025

(This article belongs to the *Special Issue: 3D-Printed Biomedical Devices*)

Abstract

Congenital heart disease (CHD) has been one of the most serious problems in newborns. For fetal heart health care, 3D modeling and printing technology have been adopted in the diagnosis of CHD during antenatal care. However, the development of 3D printing techniques and their clinical applications have been hindered by the manual processing of ultrasound (US) volume data in clinical practice. To overcome this problem, we present an interactive semi-automatic method based on deep learning that uses manual processing results from expert sonographers for training. The accuracy, interpretability, and variability of the performances were evaluated on the validation set. The results demonstrated that compared with a physician with less than 3 years of experience, a better Faster- region-based convolutional neural network-based threshold was achieved using our proposed fetal heart reconstruction technique (FRT), with enhanced performance based on the outflow tract view and three-vessel view. No significant difference was found among the clinical parameters, in proportion, measured from the model rebuilt using FRT and US volume data. Furthermore, the reconstruction time of the fetal heart blood pool model was reduced from approximately 5 h to 5 min. Our results indicate that deep learning has the ability to process US data accurately, representing an important step towards the reconstruction of the fetal heart digital model, which is critical for advancing clinical diagnosis and treatment of CHD during pregnancy.

***Keywords*:** 3D printing technology; Congenital heart disease; Deep learning; Reconstruction of ultrasound imaging data

1. Introduction

Congenital heart disease (CHD) is the most common cause of infant mortality, affecting 2.4 to 13.7 per 1000 newborns.[1] Obstetric ultrasound (US) has been the gold standard imaging method for the detection and diagnosis of fetal malformations during the antenatal period. Initially, the International Society of Ultrasound in Obstetrics and Gynecology (ISUOG) emphasized the use of four-chamber view (FCV) in fetal cardiac examinations. Subsequent guidelines introduced the outflow tract view (OTV) and three-vessel view (TVV) to visualize the overall cardiac structure for a comprehensive assessment.[2] Recent advancements in 3D US techniques have significantly enhanced the visualization of spatial structures of the fetal heart.[3] However, 3D structures cannot be comprehended thoroughly based on 2D images, which usually leads to low-efficiency treatment strategy planning for the fetus.[4]

In medical imaging, deep learning approaches have gained prominence in recent years.[5] Mofrad et al.[6] utilized deep learning to augment and assist clinicians in the automated diagnosis of adult heart diseases. Nonetheless, constructing accurate fetal heart models from US data remains challenging due to the small heart size. To address this, we employed deep learning for precise fetal heart modeling, aiding in diagnosis and prenatal screening. Moreover, 3D printing technology offers opportunities to create tangible fetal heart models, benefiting various facets of fetal healthcare such as surgeon training, personalized pre-surgical planning, and doctor–patient communication.[7–10] In this study, we employed PolyJet multi-material 3D printing due to its high resolution (~200 μm), excellent surface finish, and ability to reproduce small and complex anatomical structures such as fetal heart chambers and vessels. Compared with fused deposition modeling (FDM) or stereolithography (SLA), PolyJet offers greater accuracy and material flexibility, making it particularly well-suited for fabricating detailed fetal cardiac models for clinical and educational applications. In parallel, the integration of machine learning into additive manufacturing processes has garnered increasing attention. Zhang et al.[11] provided a comprehensive review of how neural networks and reinforcement learning are being utilized to optimize printing parameters, material formulations, and fabrication efficiency. Similarly, Li et al.[12] highlighted the role of big data and digital twin frameworks in enabling adaptive and intelligent control of 3D printing workflows. While these efforts are primarily focused on manufacturing engineering, our work addresses the upstream phase—employing deep learning to enhance the fidelity of anatomical models derived from US data, which ultimately contributes to higher-quality medical 3D printing outputs. However, the time and resources required for image segmentation pose significant limitations to the clinical application of 3D printing techniques. To address the limitations of both manual processing and existing deep learning models, we propose a semi-automatic segmentation pipeline that introduces two key innovations. Firstly, a region-limited Faster Region-based Convolutional Neural Network (R-CNN)-based position detector is applied to isolate fetal heart structures from noisy US backgrounds, reducing false positives caused by rib shadowing and organ overlap. Secondly, instead of relying solely on fully automated thresholding, the system integrates expert-in-the-loop adjustments, allowing sonographers to interactively fine-tune segmentation based on grayscale analysis. This hybrid strategy offers improved interpretability, flexibility, and clinical usability—filling a critical gap between automated artificial intelligence (AI) tools and practical medical workflow.

In this study, we introduced the fetal heart reconstruction technique (FRT) for the semi-automatic segmentation and post-processing of fetal echocardiography (Figure 1). Initially, we converted US volume scans into sequential 2D images and performed detailed frame-by-frame segmentation of the fetal heart using FCV, OTV, and TVV to train and test the R-CNN. The R-CNN then identified the fetal heart's position within the echocardiogram data and generated a segmentation mask. The FRT was subsequently employed to perform segmentation of the US images, generating results for reconstructing a basic digital model of the fetal heart. Ultimately, these digital fetal heart models were 3D printed. This method offers a semi-automated approach to rapidly reconstruct fetal heart models from US data, presenting a new diagnostic strategy for clinical fetal heart analysis.

2. Methods

2.1. Study participants

The study was approved by the Ethics Committee of the Second Affiliated Hospital of Air Force Medical University (approval no. TDLL-202402-01). All pregnant women in this study were informed of the safety and limitations of US and signed an informed consent form prior to examination. We retrospectively studied the echocardiographic volume datasets obtained by 4D US with Spatiotemporal Image Correlation from 100 normal fetuses as compulsory supervised learning cases. All of the fetuses were singletons and were selected from prenatal screening tests in the Department of Ultrasound Diagnosis at Tangdu Hospital (China) from January 2019 to May 2021.

2.2. Data acquisition

The scanning operation was strictly performed in accordance with the practice guidelines updated by the

ISUOG. All pregnant women were told to relax and lie in the supine position. Echocardiographic volume data were obtained by a Voluson E10 US system (GE Healthcare, USA [Campanella, #25]) equipped with an eM6C electric matrix transducer (2–7 MHz) to ensure that the fetus was in the supine position and its cardiac apex facing towards the front (11, 12, or 1 o'clock directions). Once data collection was initiated, the pregnant woman was told to avoid making any movement and hold her breath in order to minimize stitching artifacts. Meanwhile, principal sections, including the abdominal transverse section, the standard FCV, the left ventricular outflow tract section, the right ventricular outflow tract section, and the three-vessel section and its derivative sections, were examined strictly in accordance using the three-segment analysis method to ensure the proper condition of fetal hearts. Finally, the end-systolic phase with valves completely closed was precisely selected using M-mode; the data set was saved and output in Cartesian volume format for editing and 3D modeling.

2.3. Preprocessing of volume data into 2D images

A standard full scanned data includes 50–100 volume data, consisting of each time phase of the fetal heart. In this study, one end-diastolic volume data contained the spatial structure of the fetal heart extracted from each individual and can be decomposed into 50–70 2D images—depending on the size of the heart—spaced 0.02 cm apart from each other. All images were saved in JPEG format. According to the suggestions of ISUOG, images were divided into FCV, OTV, and TVV. To generate the label that can be trained by Deep Neural Network (DNN), the graphical image annotation tool "LabelImg" was used by professional sonographers to annotate data. A standard data stream is made up of a JPEG 2D image as data and an annotation (in XML format) as the label. The complete dataset contained 5255 data streams from 110 unique individuals. Images were randomly split into 3297, 1097, and 403 images as the training, validation, and test sets, respectively. Each image and annotation was manually rechecked by two sonographers who did not participate in the annotation of original data to confirm the reliability of the data set. The summary statistics of data are presented in Table 1.

2.4. Model development and training for fetal heart position detection

As displayed in Figure 1, FRT is an interactive method of medical image segmentation, combining both position detection and interactive binary threshold segmentation. Position detection was performed using the Faster-R-CNN architecture, which contains a feature extractor, region proposal networks (RPNs), region of interest (ROI) pooling, and a classifier.[13] A convolutional neural network (CNN) was used to extract the potential feature in the detection field during image classification, as it can accurately identify human-identifiable phenotypes and characteristics that are not recognized by human experts.[14–18] The Visual Geometry Group (VGG) CNN architecture—without complete connection and classification layers—is retrained by backpropagation and was used as the feature extractor.[19] Each image was resized to 300 × 300 pixels to ensure compatibility with the dimensions of the VGG network architecture before processing in the feature extractor. Region proposals are the output of RPN, which consists of classification and regression layers. The classification layer has a score that represents the ROI or the background, while the regression layer has four coordinates that indicate the position of the fetal heart. ROI pooling, characterized by the non-fixed size of feature maps, is used to collect region proposals generated by RPNs and feature maps, creating a vector with a similar shape to the feature map. In the classifier, bounding box regression and classification layers were used to generate a more accurate target detection box and proposal class.

For detecting the position of the fetal heart, the parameters were initialized randomly and trained using the same learning rate of 0.001, momentum of 0.9, and batch size of 16 to minimize the function loss for each object proposal. The model was trained using the training set and tested using the test set. The data were split such that the same US image was not in both training and test sets. Both training and test were performed in Python using Google's TensorFlow deep learning framework.[20] The training was terminated if the internal validation loss did not decrease for 10 epochs (early stopping criteria), and

Table 1. Summary statistics of the training, test, and validation sets

View	Training	Test	Validation	Total
FCV	1462	627	224	2313
OTV	1096	470	164	1730
TVV	739	317	156	1212
Total	3297	1097	403	5255

Note: The values in the table refer to the number of annotated 2D ultrasound images. Abbreviations: FCV: Four-chamber view; OTV: Outflow tract view; TVV: Three-vessel view.

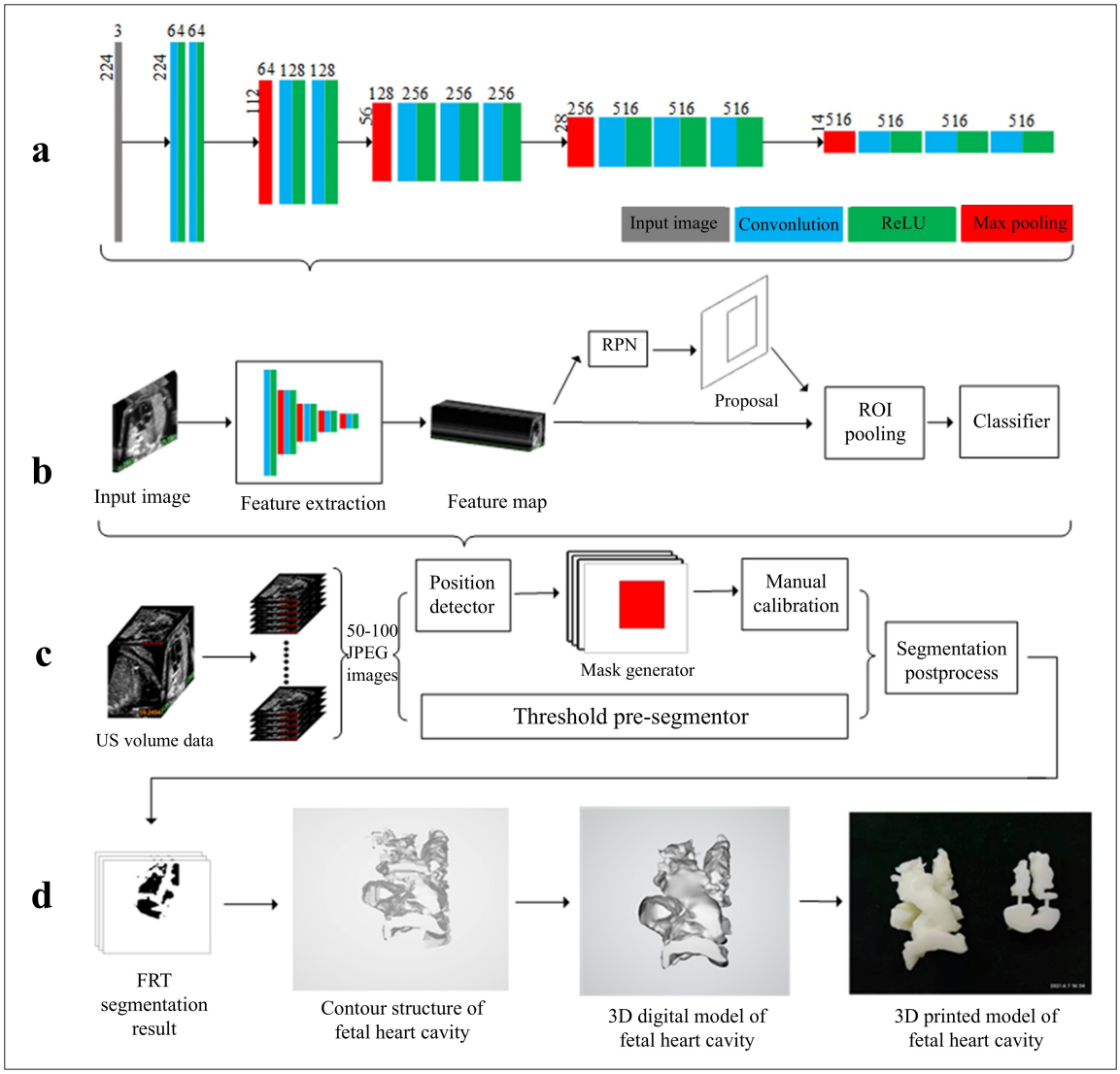

Figure 1. Workflow of reconstructing a 3D fetal heart cavity digital model using FRT. (A) Feature extraction: the number by the left of each layer represents the width and height, while the number on the top of each layer represents the depth; different colors represent different operations on the layer. (B) Position detection: feature maps generated by feature extraction were shared between the RPN and ROI pooling layer; proposals and feature maps collected by ROI pooling were sent to the classifier for classification and bounding box regression. (C) Framework of FRT: US volume data were divided into 2D images for segmentation; FRT used position detection to generate masks for the restriction segment area; manual calibration was performed to solve errors in the restriction area, and the masks were then multiplied with the binary results; finally, FRT segmentation results were obtained by post-processing. (D) Different stages of reconstructing the 3D-printed model of the fetal heart cavity (from the left to right): contour structures of the initial model, digital model after processing, and the 3D-printed model. Abbreviations: FRT: Fetal heart reconstruction technique; RPN: Region proposal networks; ROI: Region of interest; US: Ultrasound.

the maximum number of epochs was set to 10,000. All training was performed on a Linux operating system with one available P100 GPU and 16 GB RAM.

2.5. Reconstruction of fetal heart

Mimics software (Research Edition 21.0, Materialise NV, Belgium) is widely used in medical 3D printing and performs well in the analysis and segmentation of mineralized tissues, such as bones and teeth, in computed tomography and magnetic resonance imaging images. However, the threshold segmentation method provided by Mimics software is incapable of accurately distinguishing the region of the blood pool due to the influence of rib-shading occlusion and celiac region. For this reason, FRT uses AI to narrow down the area to be segmented as much as possible. Moreover, the segmentation results from FRT can be imported into Mimics software to rebuild the 3D model. A fetal heart position detector was used to identify

the segmented area that contains the entire structure of the heart, further generating the position mask. The mask is a matrix whose shape and position directly correspond to those of the image. To ensure that all subsequent operations are within the scope of the mask, all elements of the mask within the segmented area were labeled 1, while other elements were labeled 0. The restricted area was obtained by multiplying the mask with the original image; the grayscale distribution of the original image and the restricted area was calculated and plotted as curves. Sonographers could select an appropriate threshold to segment the restricted area by relying on the curves. By repeating the operation for each image decomposed from the echocardiographic volume data, the segmentation of scan data was obtained. Finally, the smoothing algorithm and seed fill algorithm were employed during the post-processing of segmentation.[21]

The fetal heart is a continuous solid body. Therefore, if the interval between adjacent layers of the image scanned by ultrasonic instrument (d) is small, it can be assumed that the images and their segmentations are similar between layers, or at least not significantly different. An end-diastolic volume data consists of coronal, axial, and sagittal raw sectioned images. Axial raw sectioned images were generated at 0.2 cm intervals and were sent to FRT for segmentation. Surface reconstruction of the entire structures of the fetal heart was simultaneously achieved by stacking the outlines of the segmentation results layer by layer. (x, y, z) is the coordinate of a point on the model, and $model\ (x, y, z)$ indicates whether the point is part of the model; 1 denotes "yes" and 0 denotes "no." The concept of similarity, $dst_i\ (x, y)$ indicates whether the point is part of the model on the 2D segmentation result of layer i from FRT. Therefore, the mathematical representation of the model is:

$$model\ (x, y, z) = dst_i\ (x, y) \tag{I}$$

where, in normal circumstances, $z = i$.

Removal of free structure and surface smoothing was performed in Mimics software during model post-processing to obtain a smoother and more intuitive digital model. Thereafter, the 3D model was printed with an SLA 3D printer (J750, Stratasys, USA) using photosensitive material.

2.6. 3D printing process

The 3D digital fetal heart models were fabricated into physical models using a Stratasys J750 PolyJet 3D printer (Stratasys, USA). This multi-material inkjet technology was selected for its capability to achieve high-resolution prints with smooth surface finishes, which are essential for accurately reproducing the intricate anatomical details of the fetal heart, such as chambers and vessels.

A key characteristic of the Stratasys J750 system is that fundamental print parameters, unlike those in many FDM or SLA systems, are largely controlled internally and are not user-adjustable. Instead, print characteristics are primarily determined by the selection and combination of photopolymer materials. For this study, a blend of flexible, rubber-like material and rigid resin was chosen. This material combination resulted in models with a Shore D hardness of approximately 60, providing a balance of structural stability and pliability. The models were printed at a high-quality setting, achieving a layer resolution of 200 μm. These properties enhance the models' utility for clinical visualization, education, and diagnostic communication.

2.7. Evaluation

To evaluate the performance of the segmentation task, the labels from the test set were used as the standard to calculate the positive prediction rate, recalling rate, mean intersection over union (mIOU), and Dice similarity coefficient (DSC). According to the standard label (sl) from experienced sonographers and segmentation result (sr), the pixel can be divided into four categories: true positive (TP; sl: 1, sr: 1), false positive (FP; sl: 0, sr: 1), true negative (TN; sl: 0, sr: 0), and false negative (FN; sl: 1, sl: 0). For the segmentation result of a single ultrasonic image, the values of TP, FP, TN, and FN are the total number of pixels of the corresponding category, respectively. Therefore, the positive prediction rate (P) and recalling rate (R) are defined as:

$$P = \frac{TP}{TP + FP} \tag{II}$$

$$R = \frac{TP}{TP + FN} \tag{III}$$

According to the prediction rate and recalling rate, the mIOU and DSC can be defined as:

$$mIOU = \frac{TP}{TP + FN + FP} \tag{IV}$$

$$DSC = \frac{2 \times TP}{\left(TP + FN\right) + \left(TP + FP\right)} \tag{V}$$

Since the assessment of performance on 2D images alone is insufficient to verify the accuracy of spatial structures of the 3D digital model, digital models rebuilt by different methods (e.g., manual reconstruction by doctors of varying experience and deep learning-based methods) were printed into physical models. The long diameter of the left ventricle (LDLV), long diameter of the right ventricle (LDRV), long diameter of the left atrium (LDLA), the transverse diameter of the left atrium (TDLA), long diameter of the right atrium (LDRA), and transverse diameter of right atrium (TDRA) were measured based on the physical model using a vernier caliper (Figure 6F). In addition, the same measurements were performed by sonographers of varying experience (junior doctor: <3 years of experience; middle doctor: 3–6 years of experience; senior doctor: >6 years of experience) on US volume data using the Voluson E10 US system. Notably, amplifying fine structures is an advantage of the 3D-printed model. Direct comparison of specific values is not scientific, as the length of each part changes with the magnification. Thus, with LDLV as the benchmark, the rest of the metrics were converted into ratios relative to LDLV. Finally, a one-way analysis of variance (ANOVA) was performed for comparisons among clinical evaluation values in proportion.

The performance of the segmentation task was evaluated using Python data analysis and manipulation tools, such as Numpy, Pandas, and Matplotlib. For evaluation of the performance of the 3D structure, one-way ANOVA was performed for comparisons among multiple groups using GraphPad PRISM 5.0. For all experiments, significance was defined as: $^{*}p < 0.05$, $^{**}p < 0.01$, and $^{***}p < 0.001$. No statistical method was used to predetermine the sample size.

3. Results

3.1. Segmentation performance

For reconstructing the 3D digital model of the fetal heart, identifying the blood pool in fetal hearts was the most important step in the process. Accuracy, interpretability, and variability were all important indicators for reconstruction. To investigate the accuracy of FRT, the mIOU/DSC of segmentations from three different views—using the thresholding method in Mimics software—were 0.242/0.381 for FCV, 0.165/0.278 for OTV, and 0.121/0.214 for TVV, respectively. Using the FRT method, there was a significant improvement in the performance from different views (FCV: 0.701/0.823; OTV: 0.681/0.809; TVV: 0.602/0.746). Furthermore, smoothing and removal of free small objects also enhanced performance based on FCV and OTV (FCV: 0.714/0.832; OTV: 0.687/0.813) after calibration. In summary, FRT performance is better based on OTV and TVV and worse based on FCV relative to segmentation conducted by junior doctors. Details of the evaluation indicators of the segmentation results using different methods are displayed in Table 2.

3.2. Interpretability of results

To further investigate the interpretability of the significant improvements achieved by the position detector, we hypothesized that it reduces the influences of noise, shadow, and other factors in US images by limiting the area of image processing. The grayscale distribution maps of the segmentation area indicated that there was a significant decrease in the number of pixels in the grayscale range of 20–40 (Figures 2 and 3).

Combined with the original images, these reduced pixels were mainly distributed in the shadow and noise of the non-target region. The recall rate of FRT significantly improved, and the positive prediction rate

Table 2. Segmentation performance of different methods

Method	FCV		OTV		TVV	
	IOU	DSC	IOU	DSC	IOU	DSC
Threshold	0.242	0.381	0.165	0.278	0.121	0.214
U-Net	0.712	0.830	0.593	0.740	0.431	0.591
Junior doctor	0.798	0.887	0.658	0.789	0.530	0.684
FRT-Default	0.701	0.823	0.681	0.809	0.602	0.746
FRT-IA	0.714	0.832	0.687	0.813	0.599	0.744

Note: IOU and DSC were used to evaluate the segmentation performance across different methods (rows); "FRT-Default" refers to segmentation by FRT using default parameters without manual interaction; "FRT-IA" refers to segmentation by FRT with manual interaction. Abbreviations: DSC: Dice similarity coefficient; FCV: Four-chamber view; FRT: Fetal heart reconstruction technique; IOU: Intersection over union; OTV: Outflow tract view; TVV: Three-vessel view.

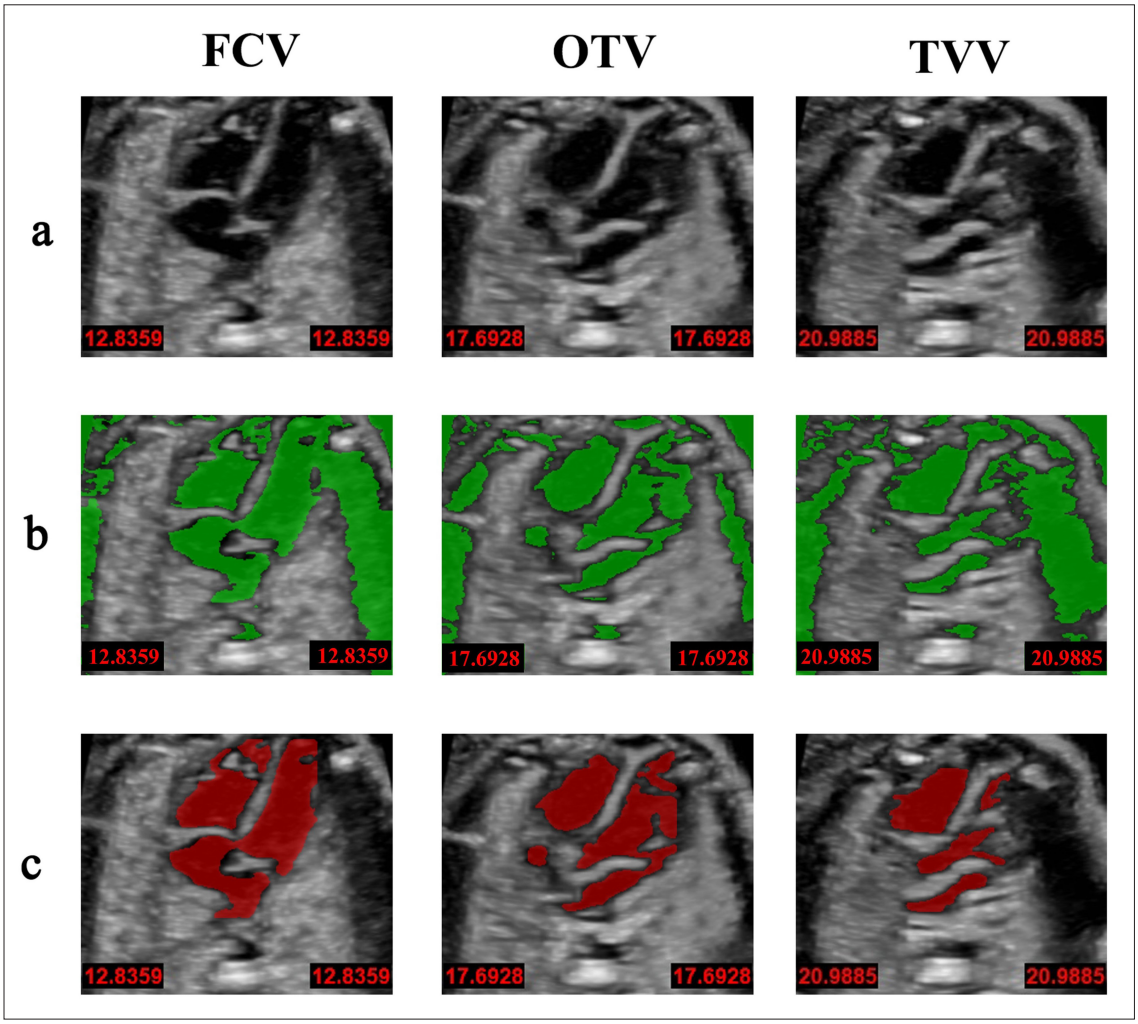

Figure 2. Examples of the segmentation results by threshold and FRT from different views (FCV, OTV, and TVV): (A) original images; (B) threshold segmentation results, and (C) FRT segmentation result. Abbreviations: FCV: Four-chamber view; FRT: Fetal heart reconstruction technique; OTV: Outflow tract view; TVV: Three-vessel view.

slightly decreased, validating our hypothesis to an extent. Although deep learning has achieved remarkable progress over the past decade, the robustness and interpretability of automated medical image segmentation have not been sufficiently addressed. To overcome the limitation, FRT used interactive image segmentation through manual correction by expert sonographers. As displayed in Table 2, the IOU and DSC of FRT from different views had advantages over that of U-Net, which is an automated method designed for fast and precise segmentation of biomedical images. These findings demonstrated that FRT had greater segmentation performance compared to U-Net.

3.3. Comparison with variation

Reconstruction of the 3D digital model relies on the segmentation results of each layer. The reliability of the 3D digital model was affected by the segmentation performance across all layers within the US volume data, making the variability of segmentation performance crucial for 3D model reconstruction. A box plot was plotted, and the standard deviations (STDs) were calculated to investigate the variability of segmentation results using different methods on the validation set (Figure 4). Compared with other methods, the variance IOU/DSC of OTV (FRT-Default: median: 0.692/0.818, STD: 0.055/0.038; FRT-IA: median: 0.693/0.819, STD: 0.069/0.051) and TVV (FRT-Default: median: 0.609/0.757, STD: 0.096/0.087; FRT-IA: median: 0.613/0.760, STD: 0.101/0.091) segmented by FRT were smaller. However, on FCV, junior doctors achieved better performance than that of FRT (median: 0.8104/0.8953, STD: 0.040/0.025). In addition, compared to FRT and junior doctors, U-Net demonstrated no

significant advantage across the three views (FCV: median: 0.6721/0.804, STD: 0.076/0.055; OTV: median: 0.654/0.791, STD: 0.142/0.138; TVV: median: 0.547/0.707, STD: 0.158/0.165). These results indicated that FRT had achieved a non-inferior performance compared with junior doctors, consistent with the results in Table 2.

3.4. Analysis of spatial structures of 3D models

All cases in the validation set were successfully rebuilt and printed using FRT to assess the accuracy of the 3D digital model and 3D-printed physical model (Figure 5). Our findings indicate that the physical model can intuitively display the spatial structures and morphologic characteristics of the blood pool in the fetal heart. Likewise, the 3D-printed physical models were well-matched with digital models, and the FRT model achieved the best accuracy among these models based on the structure of the whole heart, as well as the OTV and FCV of the fetal heart. To further investigate the accuracy

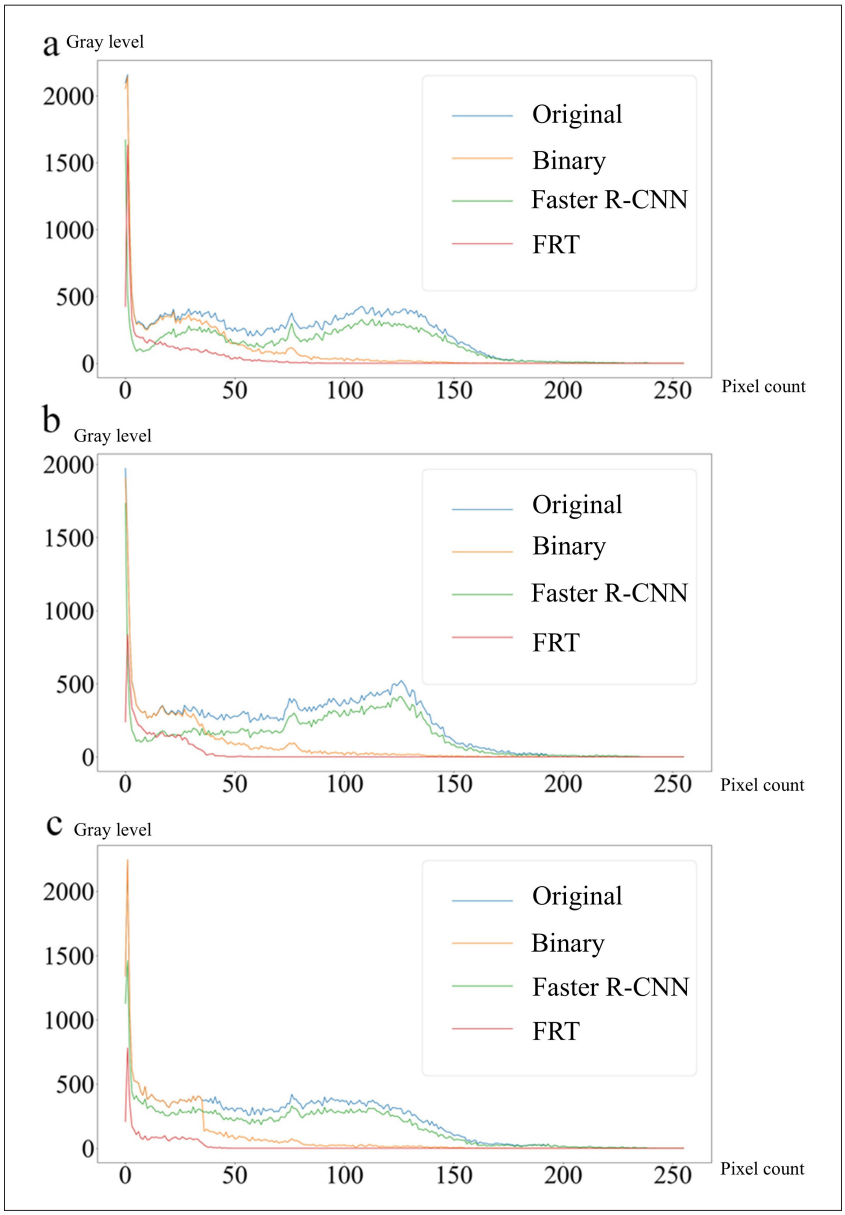

Figure 3. Grayscale distribution curves at different views: (A) FCV, (B) OTV, and (C) TVV. The blue curve represents the original image; the green curve represents the Faster-R-CNN position detector; the orange curve represents the binary threshold; and the red curve represents FRT. FRT utilized position detection to reduce the influence of noise, shadow, and other factors in US images by limiting the range of image processing. Abbreviations: FCV: Four-chamber view; FRT: Fetal heart reconstruction technique; OTV: Outflow tract view; R-CNN: Region-based convolutional neural network; TVV: Three-vessel view; US: Ultrasound.

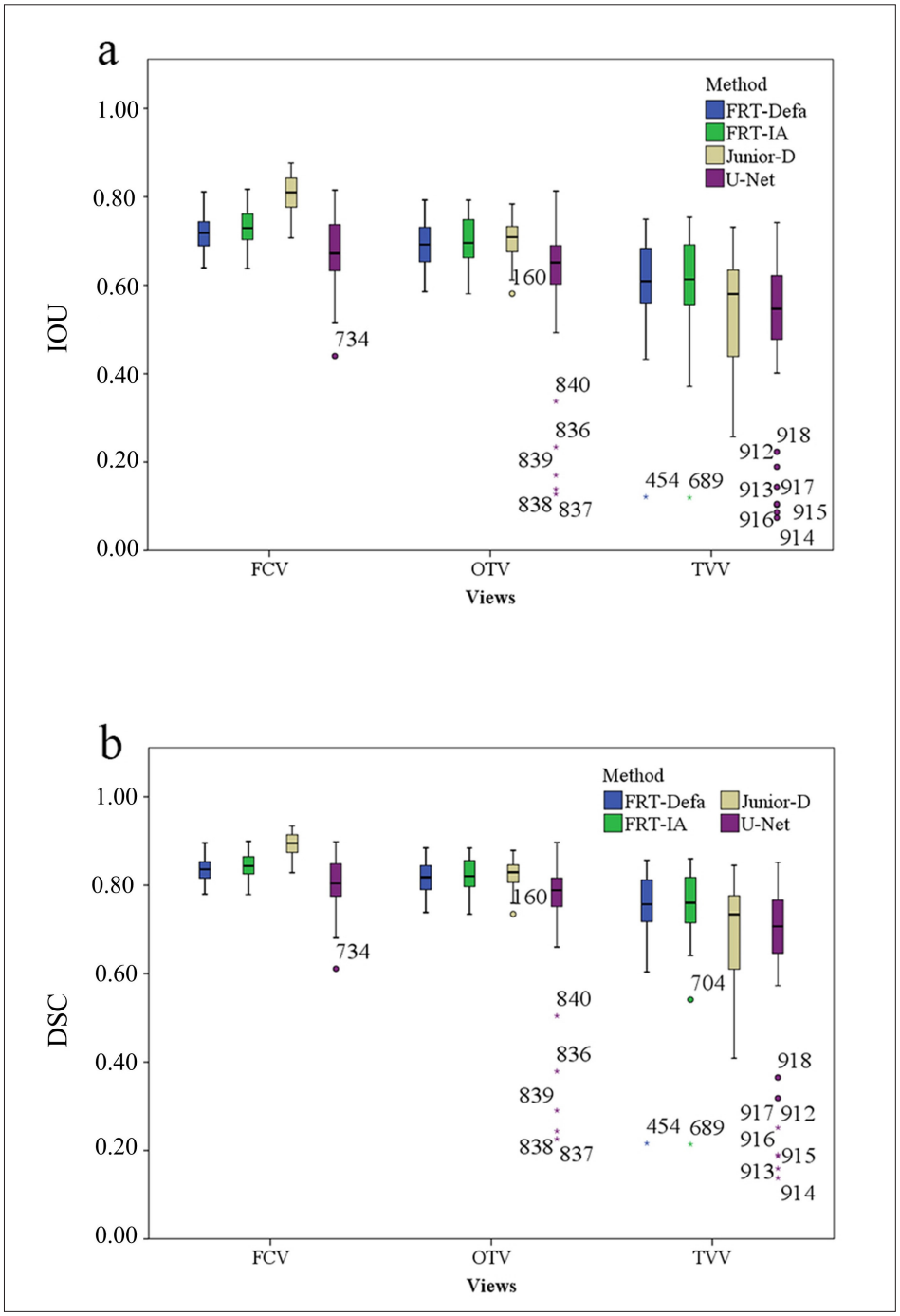

Figure 4. Variability of segmentation results using different methods. (a) Box plot of IOU variance using different methods. (b) Box plot of DSC variance using different methods. Box plots display the median as a thick line, the 25th and 75th percentiles as upper and lower bounds of the box, and individual points for data values that lie more than 1.5× the interquartile range from the median. Abbreviations: DSC: Dice similarity coefficient; FCV: Four-chamber view; IOU: Intersection over union; OTV: Outflow tract view; TVV: Three-vessel view.

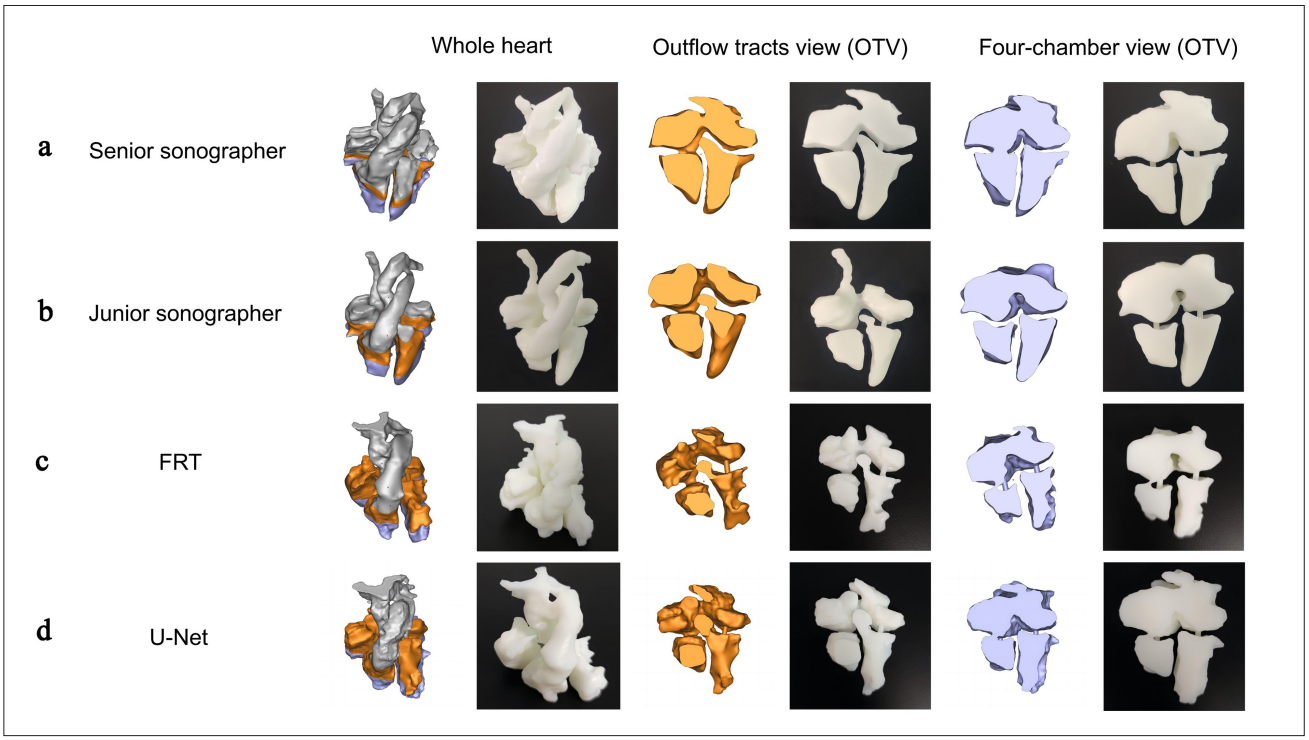

Figure 5. Examples of the 3D digital model and 3D-printed physical model of the blood pool in the fetal heart reconstructed by different methods based on the whole heart structure, OTV, and FCV: (A) manually reconstructed by a senior sonographer, (B) manually reconstructed by a junior sonographer, (C) reconstructed using FRT, and (D) reconstructed using U-Net. Abbreviations: FRT: Fetal heart reconstruction technique; OTV: Outflow tract view; FCV: Four-chamber view.

of clinical evaluation values, digital models were measured using Measure 3D Distance in Mimics software, while physical models were measured with a vernier caliper. At present, the same metrics were measured using a Voluson E10 US system with conventional 2D echocardiography to analyze the consistency among US volume data, the digital model, and the physical model. We found that there was no significant difference, in proportion, in the clinical evaluation values (LDLV, LDRV, LDLA, TDLA, LDRA, and TDRA) of US volume data measured by physicians and those measured using 3D models (Figure 6).

4. Discussion

The FRT is an advanced deep learning algorithm developed in the USA, designed to achieve cutting-edge reconstruction of fetal heart blood pool models. This groundbreaking technology combines deep learning detectors with traditional computer vision techniques to accurately segment ultrasonic images, ensuring the utmost structural precision in the resulting digital model. FRT represents a pioneering method for reconstructing fetal heart models through deep learning technology, surpassing the efficiency of human sonographers in model rebuilding. With just a single GPU, FRT enables the completion of ultrasonic image segmentation tasks for each patient within a mere minute following parameter specification. This is a remarkable improvement over the efficiency of human experts, which can take significantly longer. Consequently, FRT overcomes two major limitations in fetal heart remodeling: the time-consuming and labor-intensive nature of the process. Furthermore, FRT holds the potential to greatly benefit clinicians and patients through its applications in medical 3D printing technology.

At present, US is widely used for prenatal examinations across the world due to its relative safety, cost-effectiveness, non-invasive nature, real-time display, operator comfort, and experience.[22] However, US images have their unique limitations, including lower imaging quality, high dependence on operator or diagnostician experience, and significant variations between observers and systems used by the same observer.[23] In this context, there is a pressing need for a more objective, accurate, visual, intelligent, and integrated method for US analysis in prenatal healthcare. Deep learning has demonstrated remarkable success in medical image analysis, providing automatic tools and state-of-the-art performance.[15,17,18,24–27] Furthermore, the

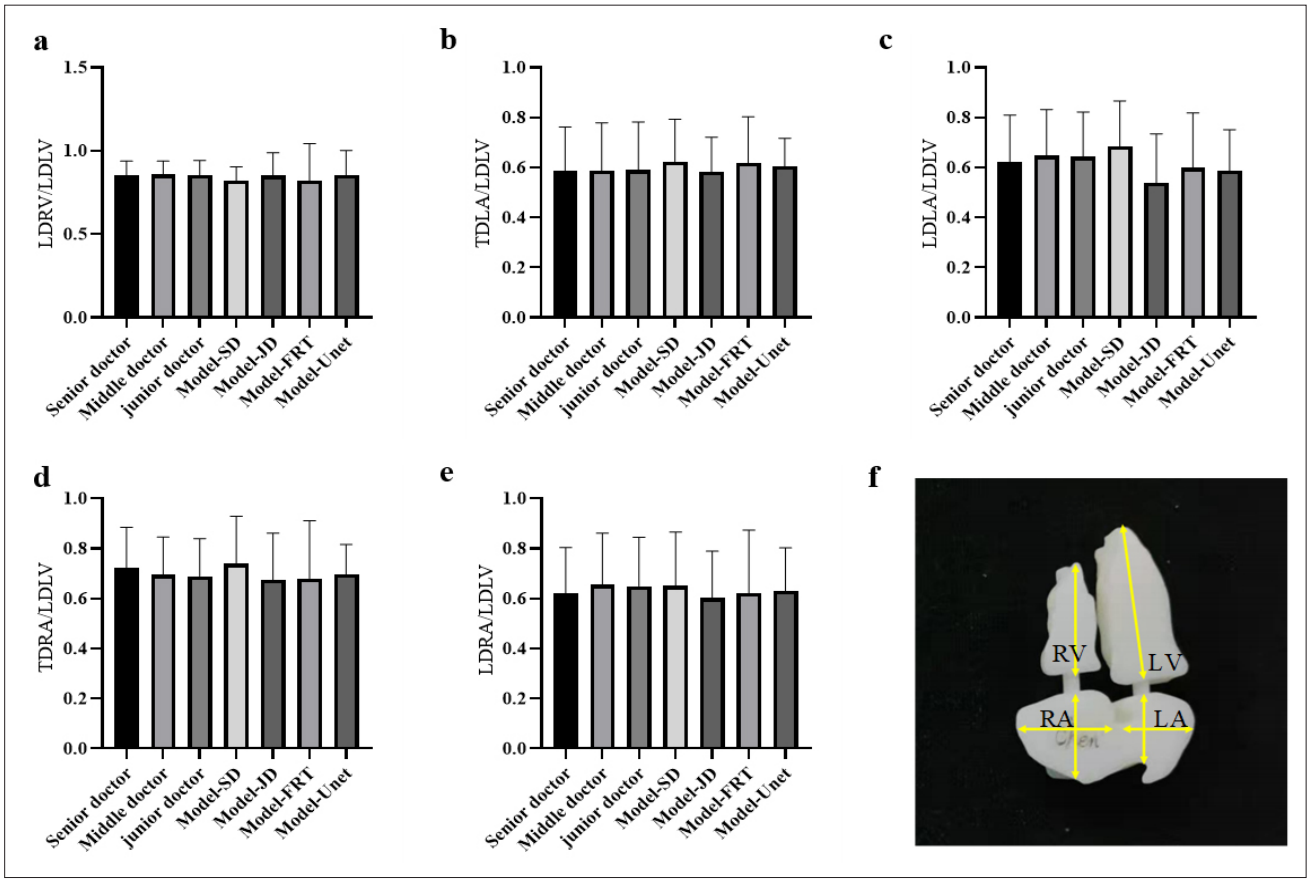

Figure 6. Variance analysis and significance test of clinical evaluation parameters (n = 3). (A) Histogram of the ratio of LDRV to LDLV. (B) Histogram of the ratio of TDLA to LDLV. (C) Histogram of the ratio of LDLA to LDLV. (D) Histogram of the ratio of TDRA to LDLV. (E) Histogram of the ratio of LDRA to LDLV. (F) Diagram of LDLV, LDRV, LDLA, TDLA, LDRA, and TDRA. Four parts are marked in the figure: the horizontal lines of the corresponding parts indicate the transverse diameters, while the vertical line indicates the long diameter. Abbreviations: LDLV: Long diameter of left ventricle; LDRV: Long diameter of right ventricle; TDLA: Transverse diameter of left atrium; LDLA: Long diameter of left atrium; TDRA: Transverse diameter of right atrium; LDRA: Long diameter of right atrium.

availability of digital models and 3D printing has opened the door to visualized prenatal examinations, offering benefits such as personalized preoperative planning, surgical simulations, enhanced medical education, and improved doctor–patient communication. Despite these advantages, 4D US scanning systems, viewable only on 2D screens, are more commonly preferred by hospitals due to the laborious and time-consuming nature of traditional manual remodeling methods.[28] FRT, however, can effectively address these limitations by semi-automating image processing tasks, thereby facilitating fast reconstruction of fetal heart models that combine seamlessly with 3D printing technology. This enables a quicker, more visualized, and intelligent approach to prenatal cardiac examination. Comparing FRT to end-to-end methods, our interactive semi-automatic algorithm offers greater flexibility and interpretability to sonographers. It allows for the adjustment of relevant parameters to enhance segmentation accuracy, granting healthcare professionals more control over the process. Moreover, the application of deep learning in this context is not merely a computational convenience, but a necessary enabler of clinical progress. The fetal heart is exceptionally small, with indistinct boundaries and low image contrast, making manual segmentation challenging and prone to variability. Traditional image processing tools are often insufficient to achieve reliable anatomical reconstruction under these conditions. FRT's integration of AI-driven detection and interactive thresholding directly addresses these challenges, demonstrating that AI can be purposefully designed to overcome domain-specific limitations, not just automate existing workflows. While the proposed FRT framework does not directly optimize 3D printing parameters, such as print path, material composition, or

support structures, its impact on the quality of printed fetal heart models is significant. By producing anatomically accurate and clean digital reconstructions with minimal noise and well-defined boundaries, FRT substantially reduces the need for manual mesh correction and improves the fidelity of 3D-printed outputs. In this aspect, the deep learning pipeline acts as an upstream quality enhancer for additive manufacturing. Therefore, future studies may explore extending AI involvement to the printing process itself—such as adaptive slicing strategies or automated printability evaluation—to further improve the efficiency and accuracy of model production.

In terms of practical workflow efficiency, FRT significantly outperforms traditional manual methods. Manual reconstruction of a fetal heart digital model typically requires clinicians to segment US volume data layer by layer from 2D slices—a labor-intensive and time-consuming process. With FRT, most segmentation tasks are automated, while clinicians can interactively calibrate the output using threshold adjustments. This semi-automatic pipeline reduces the reconstruction time for a single digital heart cavity model from approximately 5 h to just 5 min. Even without human interaction, the process can be completed in 2 min, albeit with slightly reduced accuracy. These findings demonstrate the considerable clinical value of FRT, particularly in reducing workload and enabling timely decision-making in prenatal care.

Nonetheless, FRT does have some limitations. Firstly, the size and quality of the dataset have a direct impact on the accuracy of the deep learning model. The dataset used in FRT comprises 4852 data streams from 100 unique individuals, which could potentially limit the model's performance. To address this challenge, interactive segmentation that incorporates user knowledge is integrated, resulting in a more robust segmentation performance. Secondly, while FRT significantly reduces the time required for digital model reconstruction, it is not yet capable of achieving real-time analysis of fetal heart functions. Several limitations contribute to this challenge: (i) obtaining a more robust performance through the interactive method is time-consuming; (ii) the low quality of US images and the high variation between different operators make it difficult to extract useful features, limiting the performance of end-to-end DNNs; and (iii) the limited training data available represents a bottleneck for the application of deep learning methods in prenatal US image analysis. In summary, the results of our research represent a crucial advancement in the reconstruction of digital fetal heart models using US volume data and deep learning technology. FRT significantly reduces the time and labor costs associated with reliable model construction, paving the way for the future development of real-time analysis systems based on 3D digital models, as opposed to the current 2D anatomical section-based approach. Future research efforts will focus on achieving real-time analysis of 3D fetal hearts, further enhancing the field of prenatal healthcare.

5. Conclusion

In this study, a fetal heart 3D digital model was constructed using FRT based on US volume data. The model may be used to enhance the clinical diagnosis and treatment of CHD during pregnancy. Our results indicate that deep learning has the ability to process US data accurately, representing an important step towards reconstructing fetal heart digital model and advancing clinical diagnosis and treatment of CHD during pregnancy.

Acknowledgments

None.

Funding

This work was supported by the Key Research and Development Project of Shaanxi Province (2021LLRH-08).

Conflict of interest

The authors declare that they have no competing financial interests or personal relationships that could have appeared to influence the work reported in this paper.

Author contributions

Conceptualization: Lijun Yuan, Airong Qian
Data Curation: Zekai Zhang, Zhuojun Mao
Investigation: Wenjuan Zhang, Linbin Lai
Methodology: Jiahe Liang, Zewen Zhang
Resources: Yitong Guo, Na Hou
Supervision: Tiesheng Cao, Yu Li, Lijun Yuan, Airong Qian
Writing–original draft: Wenjuan Zhang, Linbin Lai
Writing–review & editing: Tiesheng Cao, Yu Li

Ethics approval and consent to participate

This study involved human subjects and was conducted in accordance with the ethical principles outlined in the Declaration of Helsinki. The research protocol titled "Three-dimensional Fast Reconstruction in Fetal Ultrasound Imaging Using Artificial Intelligence Techniques and Three-dimensional (3D) Bioprinting" was reviewed and approved by the Institutional Review Board (IRB) of Tangdu Hospital, Air Force Medical University (approval no.: TDLL-202402-01; date: January 5, 2024).

Consent for publication

Prior to participation, all subjects provided written informed consent. The study adhered to strict confidentiality and data protection measures to ensure the privacy of participants. No additional ethical concerns or conflicts of interest were identified during the research.

Availability of data

The clinical imaging data used in this study are restricted by ethical data protection permissions and are not available for distribution.

References

1. Benjamin EJ, Muntner P, Alonso A, et al. Heart disease and stroke statistics-2019 update: a report from the American Heart Association. *Circulation*. 2019;139(10):e56-e528. doi: 10.1161/cir.0000000000000659
2. International Society of Ultrasound in Obstetrics and Gynecology, Carvalho JS, Allan LD, et al. ISUOG practice guidelines (updated): sonographic screening examination of the fetal heart. *Ultrasound Obstet Gynecol*. 2013;41(3):348-59. doi: 10.1002/uog.12403
3. Jantarasaengaram S, Vairojanavong K. Eleven fetal echocardiographic planes using 4-dimensional ultrasound with spatio-temporal image correlation (STIC): a logical approach to fetal heart volume analysis. *Cardiovasc Ultrasound*. 2010;8:41. doi: 10.1186/1476-7120-8-41
4. Huang J, Shi H, Chen Q, et al. Three-dimensional printed model fabrication and effectiveness evaluation in fetuses with congenital heart disease or with a normal heart. *J Ultrasound Med*. 2021;40(1):15-28. doi: 10.1002/jum.15366
5. Fu Y, Lei Y, Wang T, Curran WJ, Liu T, Yang X. Deep learning in medical image registration: a review. *Phys Med Biol*. 2020;65(20):20tr01. doi: 10.1088/1361-6560/ab843e
6. Madani A, Ong JR, Tibrewal A, Mofrad MRK. Deep echocardiography: data-efficient supervised and semi-supervised deep learning towards automated diagnosis of cardiac disease. *NPJ Digit Med*. 2018;1:59. doi: 10.1038/s41746-018-0065-x
7. Ackland DC, Robinson D, Redhead M, Lee PVS, Moskaljuk A, Dimitroulis G. A personalized 3D-printed prosthetic joint replacement for the human temporomandibular joint: from implant design to implantation. *J Mech Behav Biomed Mater*. 2017;69:404-411. doi: 10.1016/j.jmbbm.2017.01.048
8. Diment LE, Thompson MS, Bergmann JHM. Clinical efficacy and effectiveness of 3D printing: a systematic review. *BMJ Open*. 2017;7(12):e016891. doi: 10.1136/bmjopen-2017-016891
9. Hosny A, Dilley JD, Kelil T, et al. Pre-procedural fit-testing of TAVR valves using parametric modeling and 3D printing. *J Cardiovasc Comput Tomogr*. 2019;13(1):21-30. doi: 10.1016/j.jcct.2018.09.007
10. Costello JP, Olivieri LJ, Su L, et al. Incorporating three-dimensional printing into a simulation-based congenital heart disease and critical care training curriculum for resident physicians. *Congenit Heart Dis*. 2015;10(2):185-90. doi: 10.1111/chd.12238
11. Ng WL, Goh GL, Goh GD, Ten JSJ, Yeong WY. Progress and opportunities for machine learning in materials and processes of additive manufacturing. *Adv Mater*. 2024;36(34):e2310006. doi: 10.1002/adma.202310006
12. Jin L, Zhai X, Wang K, et al. Big data, machine learning, and digital twin assisted additive manufacturing: a review. *Mater Des*. 2024;244:113086. doi: 10.1016/j.matdes.2024.113086
13. Ren S, He K, Girshick R, Sun J. Faster R-CNN: towards real-time object detection with region proposal networks. *IEEE Trans Pattern Anal Mach Intell*. 2017;39(6):1137-1149. doi: 10.1109/TPAMI.2016.2577031
14. Bell S, Zitnick CL, Bala K, Girshick R. Inside-outside net: detecting objects in context with skip pooling and recurrent neural networks. *Proc CVPR IEEE*. 2016:2874-2883. doi: 10.1109/Cvpr.2016.314
15. Ardila D, Kiraly AP, Bharadwaj S, et al. End-to-end lung cancer screening with three-dimensional deep learning on low-dose chest computed tomography. *Nat Med*. 2019;25(6):954-961. doi: 10.1038/s41591-019-0447-x
16. Poplin R, Varadarajan AV, Blumer K, et al. Prediction of cardiovascular risk factors from retinal fundus photographs via deep learning. *Nat Biomed Eng*. 2018;2(3):158-164. doi: 10.1038/s41551-018-0195-0
17. Esteva A, Kuprel B, Novoa RA, et al. Dermatologist-level classification of skin cancer with deep neural networks. *Nature*. 2017;542(7639):115-118. doi: 10.1038/nature21056
18. Coudray N, Ocampo PS, Sakellaropoulos T, et al. Classification and mutation prediction from non-small cell lung cancer histopathology images using deep learning. *Nat Med*. 2018;24(10):1559-1567. doi: 10.1038/s41591-018-0177-5
19. Simonyan K, Zisserman A. Very deep convolutional networks for large-scale image recognition. *arXiv*. 2015. doi: 10.48550/arXiv.1409.1556
20. Abadi M, Agarwal A, Barham P, et al. TensorFlow: large-scale machine learning on heterogeneous distributed systems. *arXiv*. 2016. doi: 10.48550/arXiv.1603.04467

21. Bradski G, Kaehler A. *Learning OpenCV: Computer Vision with the OpenCV Library*. Cambridge: O'Reilly; 2008. doi: 10.1109/MRA.2009.933612

22. Bishop KC, Kuller JA, Boyd BK, Rhee EH, Miller S, Barker P. Ultrasound examination of the fetal heart. *Obstet Gynecol Surv*. 2017;72(1):54-61. doi: 10.1097/OGX.0000000000000394

23. Liu S, Wang Y, Yang X, et al. Deep learning in medical ultrasound analysis: a review. *Engineering*. 2019;5(2):261-275. doi: 10.1016/j.eng.2018.11.020

24. Ouyang D, He B, Ghorbani A, et al. Video-based AI for beat-to-beat assessment of cardiac function. *Nature*. 2020;580(7802):252-256. doi: 10.1038/s41586-020-2145-8

25. Campanella G, Hanna MG, Geneslaw L, et al. Clinical-grade computational pathology using weakly supervised deep learning on whole slide images. *Nat Med*. 2019;25(8):1301-1309. doi: 10.1038/s41591-019-0508-1

26. Litjens G, Kooi T, Bejnordi BE, et al. A survey on deep learning in medical image analysis. *Med Image Anal*. 2017;42:60-88. doi: 10.1016/j.media.2017.07.005

27. Luijten B, Cohen R, de Bruijn FJ, et al. Adaptive ultrasound beamforming using deep learning. *IEEE Trans Med Imaging*. 2020;39(12):3967-3978. doi: 10.1109/TMI.2020.3008537

28. Liaw CY, Guvendiren M. Current and emerging applications of 3D printing in medicine. *Biofabrication*. 2017; 9(2):024102. doi: 10.1088/1758-5090/aa7279